SC QUADRUPOLE AND DIPOLE

A.Mikhailichenko, Cornell University, LEPP, Ithaca, NY 14853

We are describing an SC quadrupole where the field is created not only by the poles but with the wall current distributions in equal proportions. This delivers a good field quality in all apertures allowing a compact and inexpensive design. This type of quadrupole designed for Cornell ERL could be recommended for ILC also. Dipole corrector with single-layer coil is described also.

1. Overview

There are several publications describing the SC quad design for TESLA [2] and for ILC [3] which could be useful for implementation in ERL. Design of [3] repeats earlier design described in [2]. However neither of these publications contains the field through-the-lens-integrals as function of transverse offset. Meanwhile 3D field behavior is crucial for the low emittance beams, which are ILC and ERL. On the other hand it is clear that the field generation with the poles requires precise profiling which is difficult to keep unchanged in wide specifications for feeding current.

So we chose a different approach, which allows, theoretically, a good-field region coinciding with entire aperture (100%) available for the beam [4]. Coils for this type of lens is single layered and could be manufactured with minimal efforts [5]. Numerical calculations made with MERMAID successfully used for design of CESR-C wigglers for taking into account real properties of yoke (Steel 1010).

Lenses and dipole correctors working well with 4.2^{o}K Helium; usage of Helium with lower temperature, say 2^{o}K (which is in use for RF structure) is welcomed as it allows to have the margins for current to be up to 15% higher, so operation at 2 ^{o} K might bring some cost reduction.

All setup of dipole/quadrupole cold mass wrapped by mu-metal for prevention of stray field propagation to the sensitive regions of SRF structure.

2. Concept of quadrupole lens

Let us consider a lens, which has hyperbolic poles, as required by ideal quadrupole, but the coils are flat thin ones (single layer ones) attached to the straight walls running from pole to pole, Fig.1. At the surface of the iron the boundary conditions defined by $c^2\vec{\nabla}\times\vec{B}=\mu\mu_0 c^2\cdot\vec{j}-\partial\vec{E}/\partial t$, applied to the contour, including both inside region, surface current and the iron itself.

So in that case the current must cut the tangent to the iron's surface component of the field. If we suggest for the moment, that the relative magnet permeability of the iron μ>>1 and $\mu\mu_0 c^2\vec{j} >> \partial\vec{E}/\partial t$, then we can obtain

$$\frac{\partial J}{\partial z}+\frac{\partial J}{\partial \bar{z}}=2\cdot 0.4\pi\left(\frac{\partial J_s}{\partial z}\right)\Bigg|_{z\in\partial D}, \qquad (1)$$

where in brackets, the practical units (*cm, Gs)* is used), $\frac{\partial J_s}{\partial z}$ is the transverse density of the wall current $J_s = J_s(x, y) = J_s(z, \bar{z})$, $z = x + iy$, ∂D is the boundary of region (Iron). Representing field for *2D quadrupole* field

$$\overline{B} = (-i)G_1 z = (-i)G_1 \cdot (x + iy) = 2\frac{1}{2}(\frac{\partial}{\partial x} - i\frac{\partial}{\partial y}) \cdot 0.4\pi J_s \ , \tag{2}$$

one can obtain the current distribution at the walls as the following

$$G_1 a = 0.4\pi \frac{\partial J_s}{\partial y}\bigg|_{x = a,\, y \in \partial D}, \quad G_1 a = 0.4\pi \frac{\partial J_s}{\partial x}\bigg|_{x \in \partial D,\, y = a} \ . \tag{3}$$

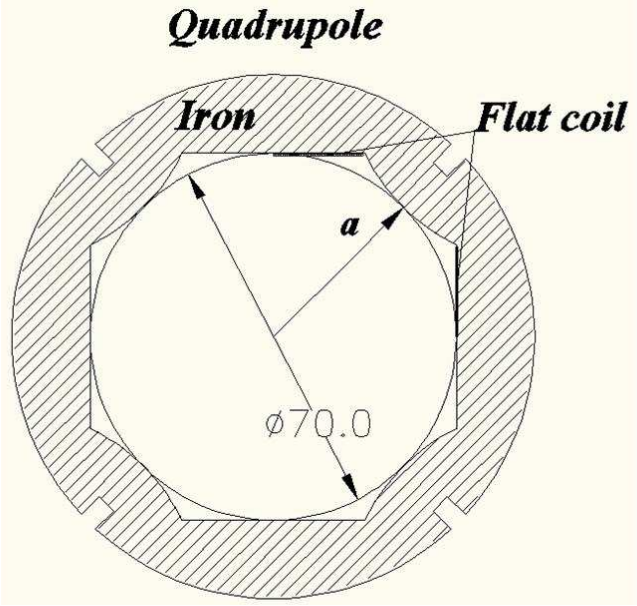

Figure 1: Concept of quadrupole. Variant with single layer coil is shown. Diameter is given in millimeters.

One can see that the *total* transverse current has a linear dependence on vertical aperture, i.e. current density is constant at this wall. For $y=a$, (upper wall) $0.4\pi \cdot J_s = G_1 a^2$. As the $G_1 a = H\Big|_{x = a}$, $J_s / a = j_s$ is the current density on the wall. Total current on the right side is $2J_s$. This gives an ideal field quality in the *entire inner region*. This kind of consideration is valid for Panofsky-Hand lens as well. Now the fraction of wall current could be replaced by iron running along hyperbolic profile. Optimal dimensions appear for the inscribing circle touching the poles and the coils.
That is the lens we are recommending for the ERL and ILC.

Maximal gradient in ERL optics could be found in MAD file is $G \cong 2T / m$, what comes to G=200 *Gauss/cm* only. So the field on the pole having radius a=3.5cm comes to $H_{\text{pole}}=Ga$=700 *Gausses*. Meanwhile the gradient could be made much higher.

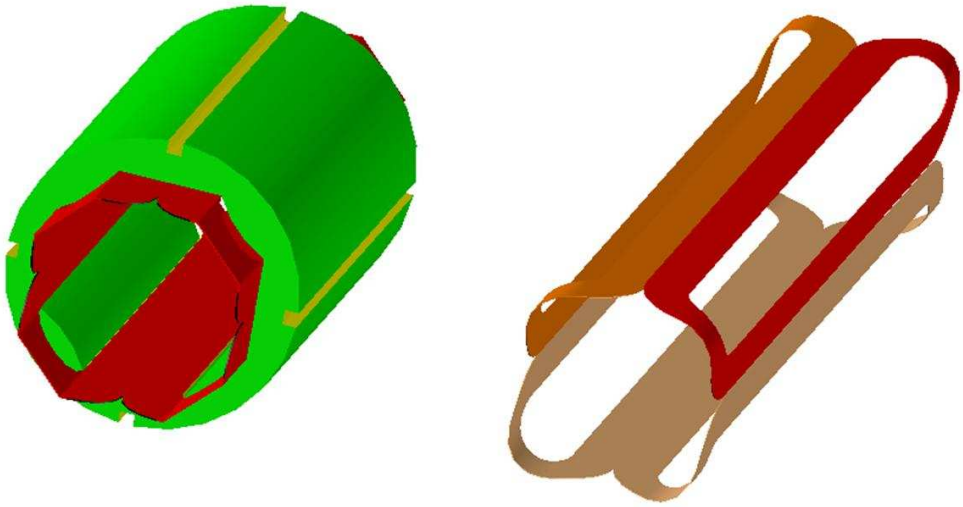

Figure 2: Isometric view of the lens cold mass (at the left) and set of four coils without iron (at the right).

Gradient defined by well known expression (practical units: *A*, *G*, *cm*)

$$\frac{Ga^2}{2} = 0.4\pi NI \;\rightarrow\quad G[G/cm] = \frac{0.8\pi NI[A]}{a^2[cm]},\ a\text{-radius (3.5 cm)}, \tag{4}$$

where a stands for the radius of inscribed circle, Fig. 1.

Table 1. Parameters of quadrupole.

(*HR*), 5GeV	16.7 *T-m*
turns per coil, N	43 (86)
Max current , *I*	220 *A*
Gradient, *G*	19.4 *T/m* (38.8)
Length/iron	0.1 *m*
$k = G/(HR)$	~1.16 m^{-2}

Naturally, for lower energy, *k* is proportionally higher. Gradient 19.4 T/m =1.94 *kG/cm* could be doubled by adding another layer in the coil.

If necessary, the second layer could be used for reduction of feeding current. One can see that for ERL case two layer coils could have feeding current as low as ~ 50A. With sacrificing of dipole corrector and usage of it space for quadrupole, the lowest current with two-layer coil could be ~10*A* only.

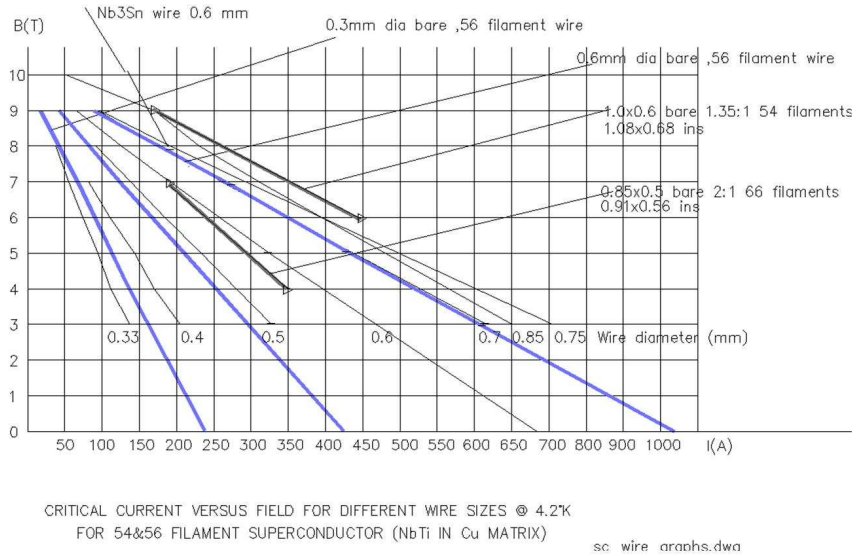

Figure 3: The wire properties at 4.2^{o}K used for calculations.

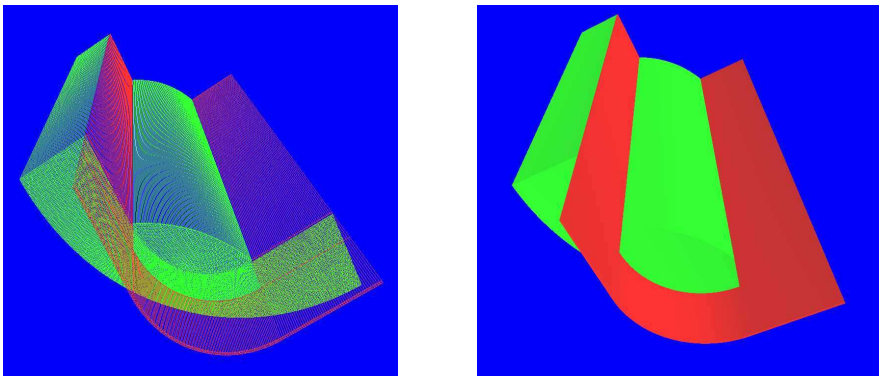

Figure 4: Model; $^{1}/_{8}$ of lens.

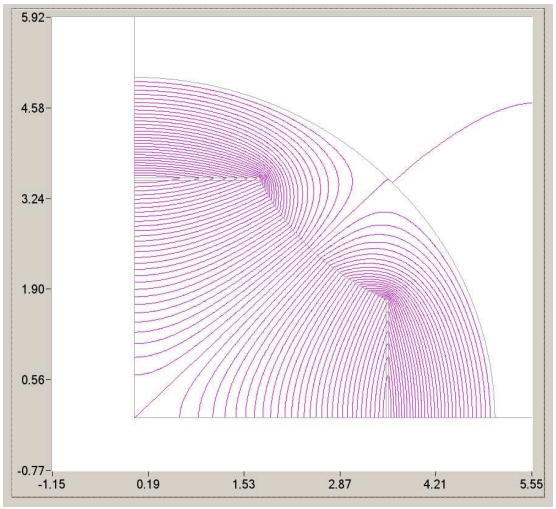

Figure 5: Field lines in quadrupole cross section.

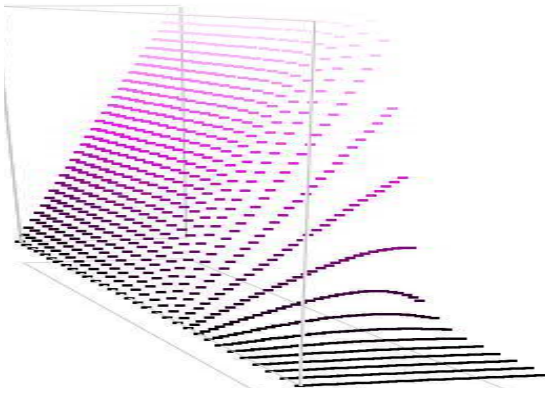

Figure 6: 3D field profile

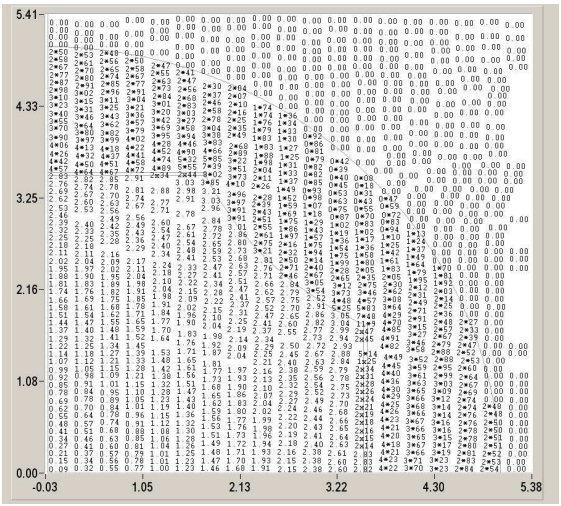

Figure 7: Numeric presentation of $|B(x,y)|$.

	An	Bn	an	bn
1	0.0000000	0.0000000	0.0000000	0.0000000
2	1.0186954	0.0000000	1.0186954	0.0000000
3	0.0000000	0.0000000	0.0000000	0.0000000
4	-0.0000005	0.0000000	-0.0000030	0.0000000
5	0.0000000	0.0000000	0.0000000	0.0000000
6	-0.0000512	0.0000000	-0.0061408	0.0000000
7	0.0000000	0.0000000	0.0000000	0.0000000
8	0.0000005	0.0000000	0.0027064	0.0000000
9	0.0000000	0.0000000	0.0000000	0.0000000
10	-0.0000066	0.0000000	-2.3972091	0.0000000
11	0.0000000	0.0000000	0.0000000	0.0000000
12	-0.0000006	0.0000000	-22.6489838	0.0000000
13	0.0000000	0.0000000	0.0000000	0.0000000
14	-0.0000173	0.0000000	107678.4512568	0.0000000
15	0.0000000	0.0000000	0.0000000	0.0000000
16	0.0000005	0.0000000	398857.3177175	0.0000000
17	0.0000000	0.0000000	0.0000000	0.0000000
18	0.0000024	0.0000000	8902211.96049	0.0000000

Figure 8: Harmonics at r=1 *cm*

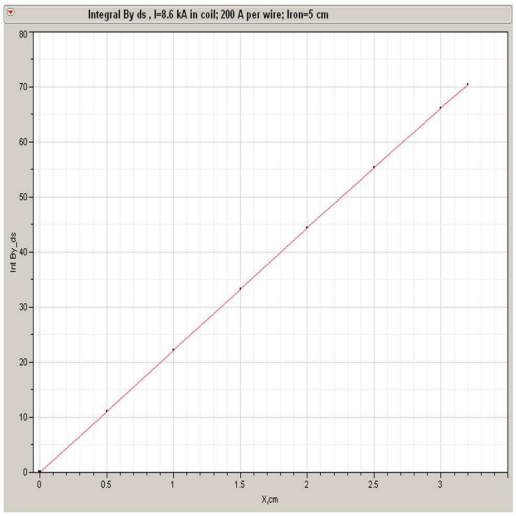

Figure 9: Integral $\int B_y(x,s)ds$, *kG-cm*,

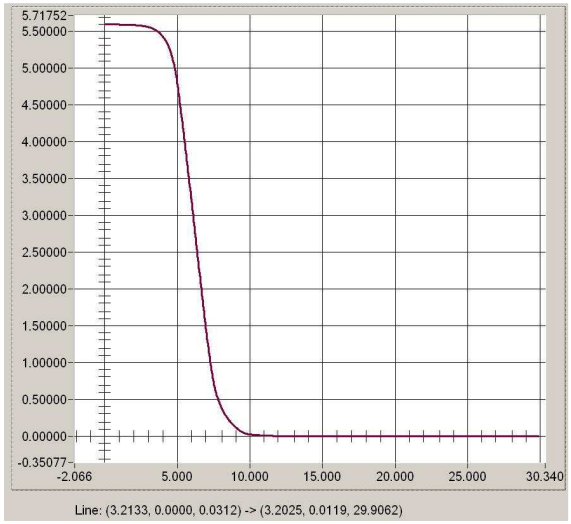

Figure 10: Field dependence on longitudinal coordinate, *kG*; transverse off-set is 3.21-cm; Iron is ±5 *cm* long.

For 200 A feeding current maximal field values at the wire is 0.25 *T* at most, Fig.7. One can see from Fig.10, that the field is dropping rapidly; at the distance 14 cm from the edge it is below 1.7×10^{-4} of its maximal value at the center.

Critical stray field value for the SRF is about 10*mT* i.e. ~100G during operation. While cooled down this value is ~1 *mT* =10*G*, even so it is at least 3 orders of magnitude bigger, than the stray field at maximal displacement. Additional end plates and wrap made from mu-metal can reduce this stray field to a negligible value. This wrap could be made from outside of quad/corrector vessel. View of model 1/8 with end plate (1/4) is represented in Figure 11.

End plates successfully used in SC wiggler design at Cornel for CESR-C project.

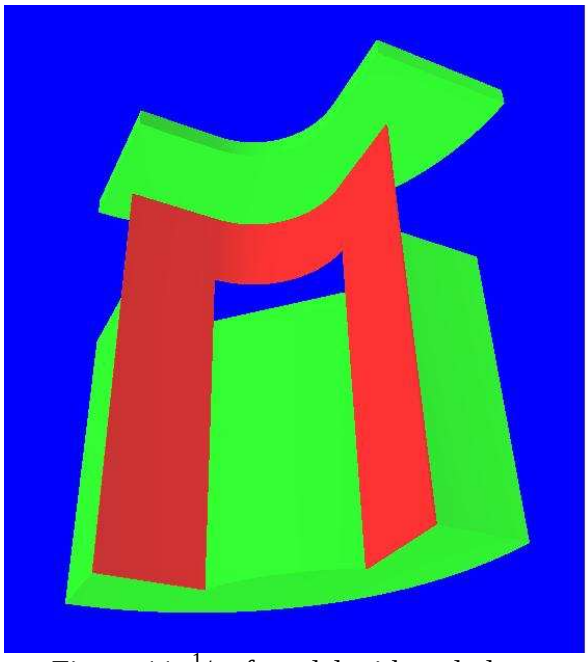

Figure 11: $^{1}/_{8}$ of model with end plate.

	X	Y	Z	Bx	By	Bz	|B|	G
3	3.20247	0.01193	19.58500	-0.000000	-0.000036	0.000000	0.000036	-0.00001
4	3.20247	0.01193	20.03375	-0.000000	-0.000033	0.000000	0.000033	-0.00001
5	3.20247	0.01193	20.48250	-0.000000	-0.000030	0.000000	0.000030	-0.00001
6	3.20247	0.01193	20.93125	-0.000000	-0.000028	0.000000	0.000028	-0.00001
7	3.20247	0.01193	21.38000	-0.000000	-0.000025	0.000000	0.000025	-0.00001
8	3.20247	0.01193	21.82875	-0.000000	-0.000022	0.000000	0.000022	-0.00001
9	3.20247	0.01193	22.27750	-0.000000	-0.000020	0.000000	0.000020	-0.00001
10	3.20247	0.01193	22.72625	-0.000000	-0.000017	0.000000	0.000017	-0.00000
11	3.20247	0.01193	23.17500	-0.000000	-0.000015	0.000000	0.000015	-0.00000
12	3.20247	0.01193	23.62375	-0.000000	-0.000013	0.000000	0.000013	-0.00000
13	3.20247	0.01193	24.07250	-0.000000	-0.000012	0.000000	0.000012	-0.00000
14	3.20247	0.01193	24.52125	-0.000000	-0.000010	0.000000	0.000010	-0.00000
15	3.20247	0.01193	24.97000	-0.000000	-0.000009	0.000000	0.000009	-0.00000
16	3.20247	0.01193	25.41875	-0.000000	-0.000008	0.000000	0.000008	-0.00000
17	3.20247	0.01193	25.86750	-0.000000	-0.000007	0.000000	0.000007	-0.00000
18	3.20247	0.01193	26.31625	-0.000000	-0.000006	0.000000	0.000006	-0.00000
19	3.20247	0.01193	26.76500	-0.000000	-0.000006	0.000000	0.000006	-0.00000
20	3.20247	0.01193	27.21375	-0.000000	-0.000005	0.000000	0.000005	-0.00000
21	3.20247	0.01193	27.66250	-0.000000	-0.000005	0.000000	0.000005	-0.00000
22	3.20247	0.01193	28.11125	-0.000000	-0.000004	0.000000	0.000004	-0.00000
23	3.20247	0.01193	28.56000	-0.000000	-0.000004	0.000000	0.000004	-0.00000
24	3.20247	0.01193	29.00875	-0.000000	-0.000004	0.000000	0.000004	-0.00000
25	3.20247	0.01193	29.45750	-0.000000	-0.000004	0.000000	0.000004	-0.00000
26	3.20247	0.01193	29.90625	-0.000000	-0.000004	0.000000	0.000004	-0.00000

Figure 11: Field (*kG*) at *z*-distance ~19-30 *cm* from center of quadrupole

One can see that field drops below 10 *mG* at *z*-distance ~24.5 *cm* from center (Quad Iron ends at 5 cm from center). End plate located at 9.5 cm from center and has a thickness 4 *mm*. It is interesting that magnetic field of 100 *mA* DC current in ERL will generate magnetic filed at iris of SRF structure the DC field

$$H \cong 2 \cdot \frac{0.4\pi \cdot I}{2\pi r} = 2 \cdot \frac{0.4\pi \cdot 0.1}{2\pi 3} = \cdot \frac{0.4 \cdot 0.1}{3} \cong 13mG,$$

where it was substituted 3 *cm* for the radius of iris diaphragm, factor 2 reflects the fact that in SRF sections two beams are running together (the accelerated one and decelerated one). Pulsed magnetic field is substantially higher, which defined by ratio of the RF wavelength and the bunch length; however the spectral components of magnetic field is two times DC one for each harmonics.

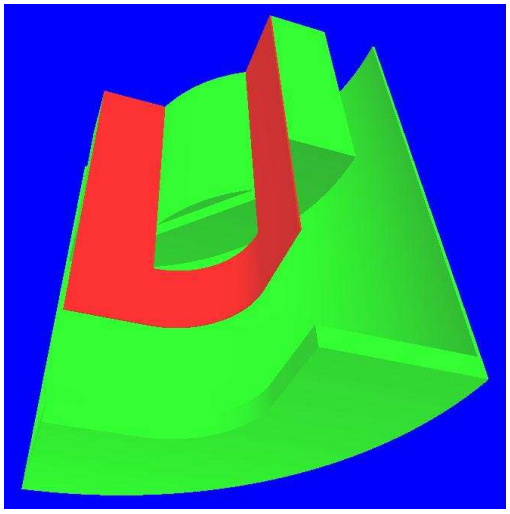

Figure 12: $^1/_8$ of model with end plate and wrap. Pole fringe cut is visible here also.

Installation additional wrap around whole lens (Fig.12) does not change distant field as the distant field determined by exponential decay of field starting from the fringe.

Table 2. Field integral as function of transverse position (Fig.9)

x, cm	$\int B_y ds$, *kG-cm*
0	0
0.5	11.0397
1.0	22.0783
1.5	33.1144
2.0	44.1390
2.5	56.1184
3.0	65.9397
3.2	70.1743

Analytical formula which approximates the integral dependence on transverse coordinate is

$$\int B_y(x,s)ds\,[kG \cdot cm] = 22.0796 \cdot x - 0.000497 \cdot x^5 - 8.9431 \cdot 10^{-6} \cdot x^9, \qquad (5)$$

where *x* measured in *cm*, feeding current is 200 A in 43-turn single layer coil (8.6 kA per coil total).

Slight deviation from linearity could be compensated by trimming the radius of pole if necessary. Parameter for trimming is pole radiuses, approximating hyperbola. By changing radius one can change the content of higher harmonics.

4. The concept of dipole corrector

For the dipole corrector a single-layer coil is chosen similarly to the quadrupole. We suggested using winding topologically confined in inner region (inside the iron frame) as this gives minimal stray fields outside the corrector.
Again, 3D modeling carried with MERMAID; yoke–Steel 1010.

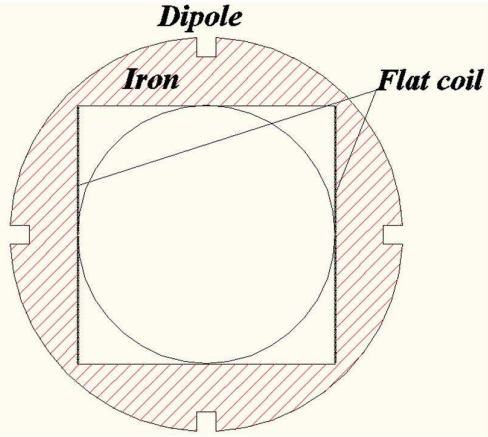

Figure 13: The concept of dipole corrector.

Figure 14: The set of saddle-type coils for one coordinate.

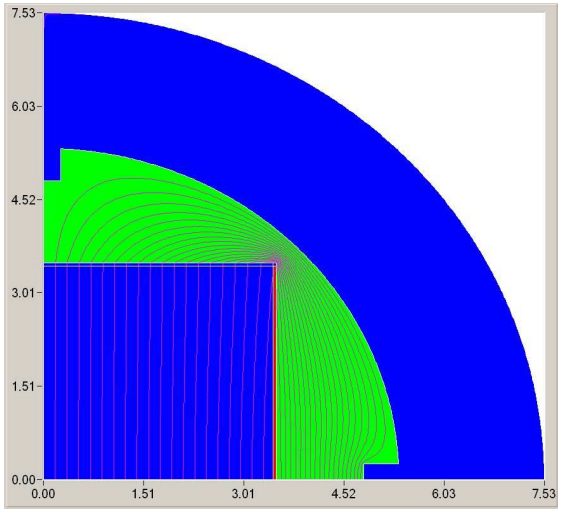

Figure 15: Field lines at the center.

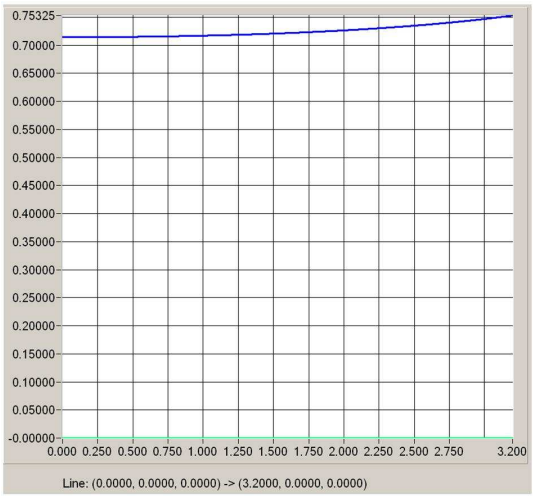

Figure 16: Field across the aperture at the center for 2kA per coil.

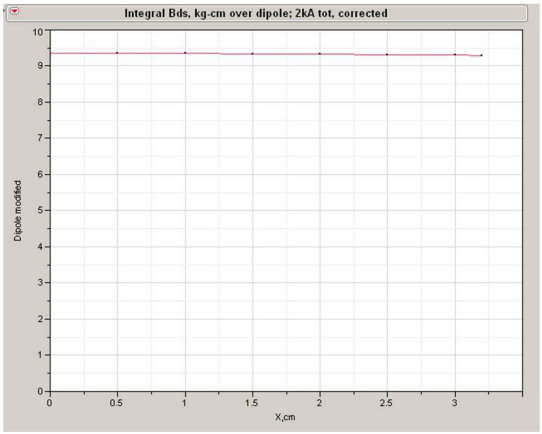

Figure 17: $\int B_y(x,s)ds,\ [kG\cdot cm]$

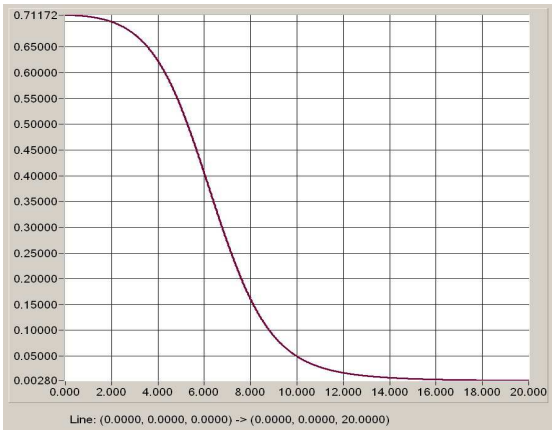

Figure 18: Longitudinal dependence of field. $B_y(x=0,s)$, s_{max}=20 cm

Table 3. Field integral as function of transverse position (Fig.17)

x, cm	$\int B_y ds$, *kG-cm*
0	9.3493
0.5	9.3484
1.0	9.3457
1.5	9.3410
2.0	9.3332
2.5	9.3205
3.0	9.3018
3.2	9.2949

Despite the field at central region increases with offset increase (Fig.16), the integral, indeed behaves in opposite way, Fig.17. That is a result of fringe field dominant action.

Analytical formula which approximates the integral dependence on transverse coordinate is

$$\int B_y(x,s)ds\,[kG\cdot cm] = 9.3493 - 0.0034\cdot x^2 - 1.98\cdot 10^{-4}\cdot x^4, \qquad (6)$$

where x measured in *cm*, total current is 2 kA per coil (~20A in single wire).
Angular kick provided by dipole for 5-GeV beam is

$$\alpha \cong \frac{\int B_y(x,s)ds\,[kG\cdot cm]}{(HR)[kG\cdot cm]} = \frac{9.35}{1.67\cdot 10^4} \cong 0.56\ mrad \qquad (7)$$

Parameters for trimming: height of the coil. By reducing the height slightly one can increase the field growth rate in Fig.16.

5. BPM

Few types could be suggested here –traditional button type, Fig. 20 and the one which uses location of BPM coils behind a thin Stainless steel wall, Fig. 21, [6], [7].
Button-type BPMs allow current and position monitoring. They could be made pretty fast with appropriate electronics. BPM behind thin StSteel foil wall allow readings averaged over time scale, depending on the thickness of the foil, which might be a microsecond level for typical case.

Nor of these types allow distinguishing between the energy of the particles. In some ERL scenario for multi-turn usage of SRF structure, two bunches of different energy might be present at the ~same location, however. The only way to distinguish the readings of current for bunches with two (and more) distinct energies E_1, E_2 might be a usage of spontaneous radiation in a (weak) undulator, Fig.19. Undulators $U_{1\text{-}4...}$ could be turned on one by one. Grating G in Fig.22 serves for separating photons having different energies.

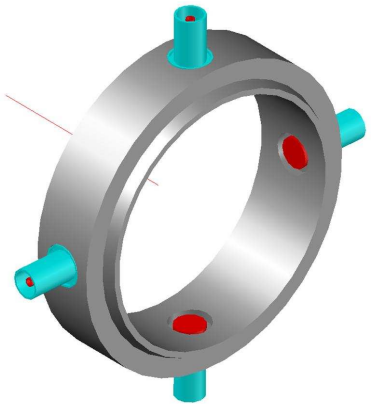

Figure 20: The button-type BPM.

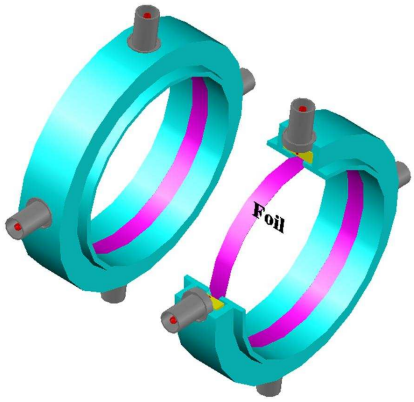

Figure 21: BPM behind thin StSteel foil wall.

With helical windings applied to the inner tube from the Helium side, one can expect for the L~400 mm available and diameter D=70 mm the undulator with the number of periods ~5 for period $\lambda \cong 70$mm. The K-factor one can expect here is $K = \frac{eH\lambda}{2\pi mc^2} \cong 0.01$. The number of photons radiated by each electron here comes to ($\alpha = e^2/\hbar c \cong 1/137$)

$$N_{\gamma 1} \cong \frac{4\pi}{3}\alpha K^2 \frac{L}{\lambda} \cong 0.002\,\alpha \cong 1.4\cdot 10^{-5}, \qquad (8)$$

delivering total number of photons for 77-pC bunch ($N_b \cong 4.8\cdot 10^8$) to $N_\gamma \cong 6700$ per bunch.

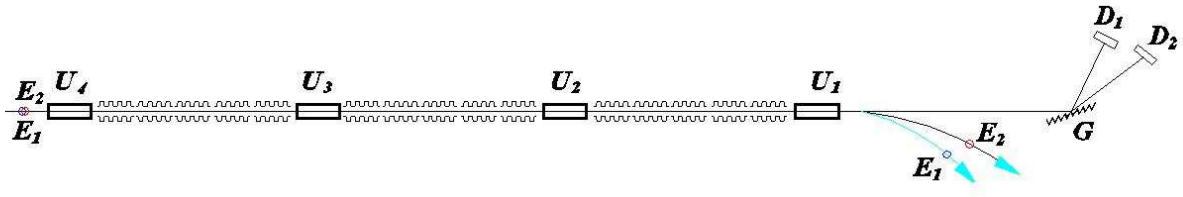

Figure 22: Possible arrangement of BPM with undulators for distinguishing parameters of beams composed with few bunches having different energies. D_1 and D_2 stand for the photon counters, G is the crystal grating.

For the sequence of bunches with f=1.3 *GHz* this brings the total number of photons per second to the

$$N_\gamma / \sec ond \cong N_\gamma \times f \cong 6.7 \cdot 10^3 \times 1.3 \cdot 10^9 \cong 8.7 \cdot 10^{12}. \quad (9)$$

The energy of radiated photons defined by

$$E_\gamma \cong 237 keV \frac{(E_b / 5GeV)^2}{(\lambda / 1mm)(1+K^2)} \cong 23.7 keV \frac{(E_b / 5GeV)^2}{\lambda / 10mm} \cong 3.4\text{keV} \quad (10)$$

for 5-*GeV* beam. For 2.5-*GeV* beam this number comes to ~0.84 keV, so the energies distinguished well. Statistics associated with these flux is well beyond the one could be well registered.

This type of monitor requires installation of registering equipment for the photons after the bend. Each undulator can be turned on/off by special sequence, so the signals from each undulator could be recognized well. Few undulators at the time also might be possible as the bunch energy change between two undulators might be substantial and allow few distinct frequencies to be resolved.

All photons radiated in a cone with angular divergence $\vartheta \cong 1/\gamma$ so radiation touches the wall at the distance $\sim \gamma D \cong 700$ meters, so this is more than enough for accurate transport the gamma flux out of vacuum chamber in the region near the turn. For reading position of the bunch the undulator must be a helical-quadrupole one. This type of undulator has zero field value at the axis. So the dipole/quadrupole undulator could be considered as additional type of BPM.

6. Installation in cryostat.

As we have already mentioned, the lens and corrector are working at 4.2^{o}K in liquid Helium bath. However as the cryostat holds 2^{o}K Helium for improvement of SRF properties of accelerating structure, operation in 2^{o}K Helium is quite desirable (but not necessary). HTS leads coming out of lens/dipole module run to the shield supported on intermediate temperature ~77^{o}K. Typical heat leak for 200A current HTS lead comes to 20mW/lead between 77–4.2^{o}K and for the leads with physical length 150mm. So total heat leak from low temperature end could reach 0.08-0.1 W/package, taking into accounts that quads required two leads and that the dipole corrector also runs at full power and for two dipole correctors two leads are in use (each dipole has one common with quadrupole). The HTS leads could be wrapped by mu-metal cylinder for protection against stray fields propagating towards the SRF structure also.

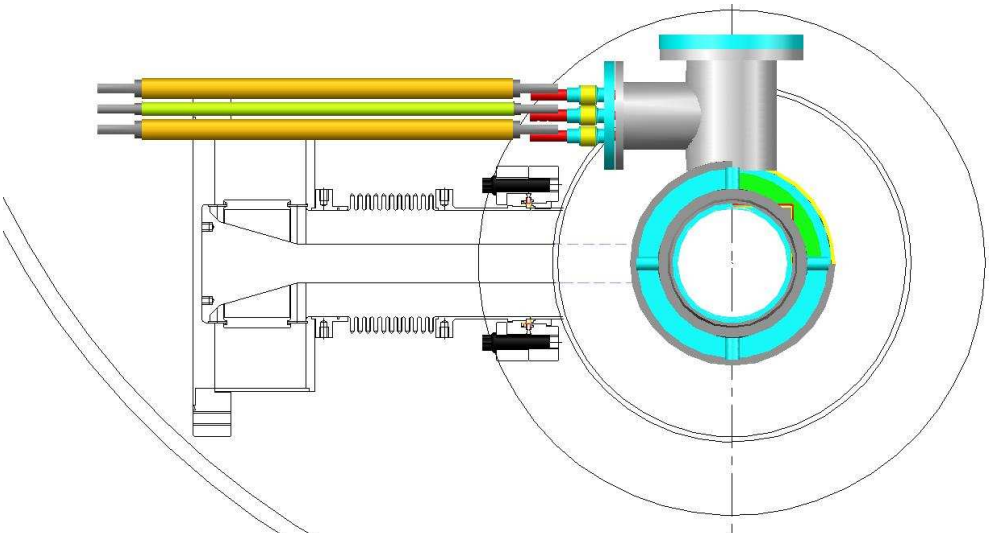

Figure 21: SC lens and dipole corrector location in cryostat. HTS leads run to 77^{o}K shield.

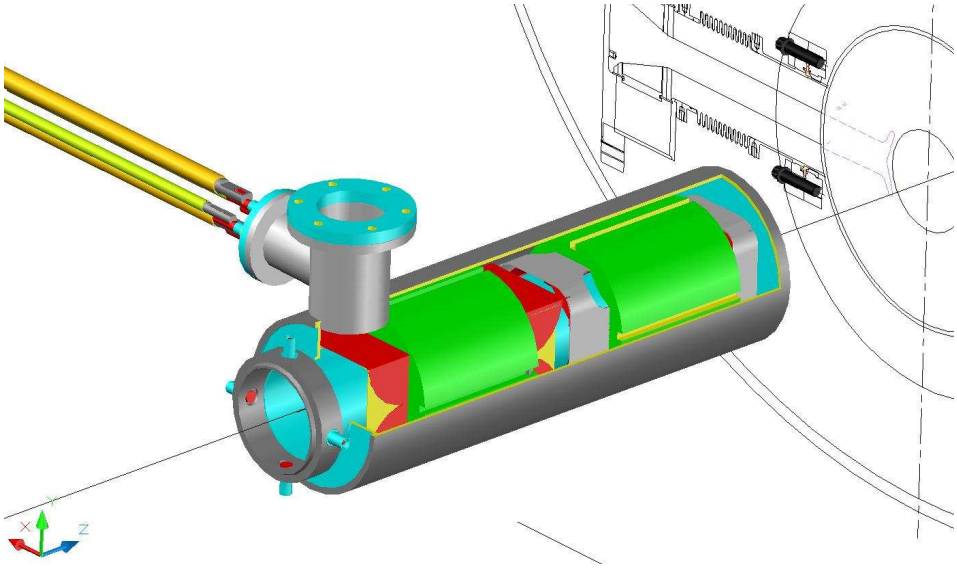

Figure 22: The lens and corrector in Helium vessel. HTS leads are seen at the left. Button-type BPM welded at the front. Longitudinal size of Quad/Dipole/BPM assembly is ~400 mm.

Quadrupole lens shown in Fig.22 located closer to RF structure as the field of quadrupole drops faster, than the field of dipole, although these magnets could be swapped.

Quad/Dipole vessel is rigid enough to be attached to the SRF vessel by flanges, which in this case can hold Quad vessel in place, in this case no additional supports required.

The Quad and Dipole corrector could be made in absolutely separate vessel, which could be inserted on central vacuum tube. The last should be equipped with removable flange. Lot of designs for such flanges exists (either with thread or with special removable enclosures).

7. Summary

Developed quadrupole and dipole occupy less than 400 *mm* of longitudinal space. This type of lens and the dipole could be recommended for usage in ILC as well. By doubling the number of turns one could reach gradient ~39 *T/m*.

Undulator-type windings could be considered as additional BPM type. For ERL with return bends there will be not a problem to acquire radiation from these undulators, located at (each) dipole/quadrupole section. For ILC the presence of chicane for installation of positron conversion system undulator allows acquiring radiation from many downstream ones also.

8. References

[1] ILC and ERL Baseline documents available at corresponding websites.

[2] A.Koski, R.Randemann, S.Wolf, "*Superconducting Magnet Package for TESLA Test Facility*", IEEE Transactions on Magnetics, Vol. 32,No4, July 1996, pp 2155-2158.

[3] V.S.Kashikhin, N.Andreev, M.J.Lamm, M.L.Lopes, J.C.Tompkins, A.V.Zlobin,"*Design and Manufacturing Main Linac Superconducting Quadrupole for ILC at FERMILAB*", IEEE Transactions on Magnetics, Vol. 18, No 2, June 2008, pp 155-158.

[4] A. Mikhailichenko, "*3D Fields. Representation and Measurements*", (Cornell U., LNS), CBN-95-16, 1995. 42pp.

[5] A. Mikhailichenko, T. Moore, "*Simple Procedure for Superconducting Coil Winding*", Presented on PAC2001, June 18-22, Chicago, IL, RPPH 319, Proceedings, pp. 3645-3647.

[6] A. Mikhailichenko, "*A Sensor of the Current Coordinates and Current of an Intense Microwave Modulated Beam*", Instrum.Exp.Tech.27:414-416,1984, Prib.Tekh.Eksp.N2:149-150,1984.

[7] A.Alexandrov, S.Heifets, A.Novokhatsky, "*Simple Low-Frequency Beam Pickup*", Phys. Rev. ST Accel. Beams 11:114401,2008; SLAC-PUB-13130, Mar 25, 2008. 20pp.